The Nature of Conduction Pathways in Mixed Alkali Phosphate Glasses

Andreas Hall[1], Stefan Adams[2] and Jan Swenson[1]

[1]Condensed Matter Physics, Department of Applied Physics, Chalmers University of Technology, S-412 96 Göteborg, Sweden, E-mail: A. Hall: andreash@fy.chalmers.se; J. Swenson: f5xjs@fy.chalmers.se

[2]GZG, Abt. Kristallographie, Universität Göttingen, Goldschmidtstraße 1, D-37077 Göttingen, Germany, E-mail: sadams@gwdg.de;

Abstract. In this paper we discuss the nature of the ion conduction pathways in $Li_xRb_{1-x}PO_3$ glasses. Our investigations are based on a bond valence analysis of reverse Monte Carlo (RMC) produced structural models in quantitative agreement with neutron and X-ray diffraction data. In a previous letter [11] we have shown that this approach enables us to reproduce and understand the mixed alkali effect (MAE) directly from the structural models. The results have shown that the drastic drop of the conductivity for an intermediate composition ($x \approx 0.5$) is mainly caused due to the blocking by immobile unlike cations, which is highly effective since the two types of alkali ions are randomly mixed and have distinctly different conduction pathways of low dimensionality. Here, we explore the local dimensionality of the pathways and discuss its implications for the network of pathways and the related ionic conductivity.

1. Introduction

In order to understand the conduction mechanism in ion conducting glasses it is essential to elucidate the microscopic structure and the nature of the conduction pathways. Basically, there are two main goals; to understand how the microscopic structure influences the ionic conductivity and to determine how the ions are actually moving on a microscopic length-scale. Both these goals are difficult to reach by purely experimental studies, since no experimental technique is able to provide a complete "picture" of the structure or any clear insight on how the ions are moving. Diffraction techniques, such as neutron and X-ray diffraction, can provide general information about the microscopic structure and from ac conductivity measurements some insights about the ion jump process can be gained. However, for a more detailed understanding of how the structural and conductivity properties are related different types of modelling techniques are used. The probably most used modelling technique is molecular dynamics (MD) simulations, which is a powerful method since it gives both structural and dynamical information, and can therefore provide a link between the microscopic structure and the conductivity properties. A limitation with the MD method is that it is usually difficult to obtain accurate model potentials for chemically complicated systems, such as ion conducting glasses. Due to the limited speed of computers it is also difficult to study the motion of ions on time-scales exceeding a few nanoseconds. Therefore, in this study we have used a different and complementary approach and produced reverse Monte Carlo (RMC) [1,2] structure models of mixed alkali phosphate glasses, which are in quantitative agreement with both neutron and X-ray diffraction data, as well as other structural and chemical knowledge of the glasses. The structure and dimensionality of the ion conduction pathways has, thereafter, been analysed by the bond valence method [3-5].

It is well known that a mixing of alkali ions gives rise to a dramatic drop in conductivity compared to the conductivities of the two corresponding single alkali glasses (see Fig. 1), and in order to understand the conduction mechanism in any ion conducting glass it is essential to also understand the reason for this conductivity drop. In fact, it is possible to gain additional

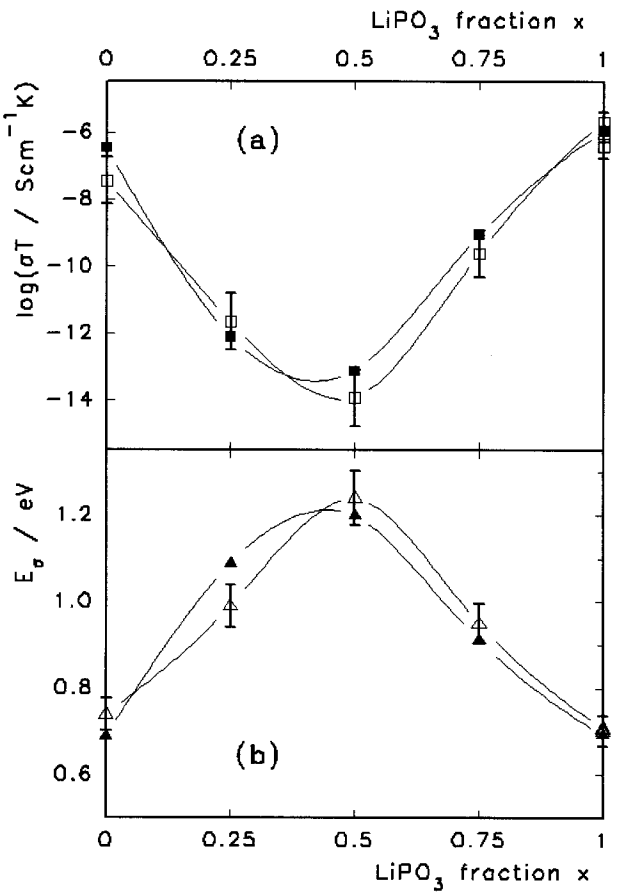

Fig. 1. dc conductivity σ_{dc} and activation energy E_σ versus composition for the glass system $Li_xRb_{1-x}PO_3$ at 300 K. Open symbols are experimental data points, taken from Ref. 28, and filled symbols correspond to the values predicted from the pathway volume fractions F of the structural models. The solid lines are guide to the eye.

knowledge about ion conduction in glasses by studying this phenomenon in mixed alkali glasses, which commonly is denoted the mixed alkali effect (MAE) [6-8].

As mentioned above, the MAE refers to the large changes in many dynamic properties that occur for ion conducting glasses when a fraction of the mobile ions is substituted by another type of mobile ions. The effect is not restricted to alkali ions, but occurs also for mixtures of other types of mobile ions. Therefore the effect is more generally referred to as the mixed mobile ion effect. The largest deviations from linearity, when the concentration ratio between the two mobile ions is changed, are observed in those properties which are related to ionic transport, such as ionic conductivity, ionic diffusion, dielectric relaxation and mechanical loss and internal friction. Macroscopic properties such as molar volume and density, refractive index, thermal expansion coefficient and elastic moduli usually change linearly or only slowly with composition. Properties related to structural relaxation, such as viscosity and glass transition temperature, usually exhibit some deviations from linear behaviour, although deviations from linearity are observed also for mixed glass-forming systems, which do not contain any mobile ions.

In the last fifty years several models (see Isard [6] and Ingram [8] for reviews) have been proposed to explain the MAE. However, it is not until recently substantial understanding of the MAE has been gained. This understanding is mainly obtained from MD simulations [9,10] and RMC modelling with [11] and without [12] the bond valence analysis of the conduction pathways. These computational methods have shown that the main reason for the MAE is that the two types of mobile ions have distinctly different conduction pathways, due to a large site mismatch energy for A ions on B sites and vice versa. Since the two types of ions are randomly mixed this implies that the A ions cause an effective blocking of the pathways for the B ions and vice versa.

2. Reverse Monte Carlo Modelling

In this study we have explored the nature of the conduction pathways in the mixed alkali phosphate glasses $Li_xRb_{1-x}PO_3$ (x = 0, 0.25, 0.5, 0.75 and 1) by means of bond valence analysis. However, this method requires accurate structural models of the glasses, which can be obtained by the reverse Monte Carlo (RMC) modelling technique [1,2]. The RMC method produces three-dimensional structural models of disordered or complex materials in quantitative agreement with diffraction, EXAFS and NMR data, as well as additional bonding constraints based on other experimental or chemical knowledge [13-17]. In this case the RMC modelling was based on neutron and X-ray diffraction data that were obtained at the liquid and amorphous diffractometer (LAD) [18] at Rutherford Appleton Laboratory, UK, and on the GILDA instrument [19] at the European Synchrotron Radiation Facility (ESRF), Grenoble, France. The experimental procedures and data corrections are described in detail elsewhere [17,20].

In order to obtain chemically sensible structures in agreement with previous structural findings from e.g. NMR [21] and Raman scattering [22] experiments we used coordination constraints for the P-O network.

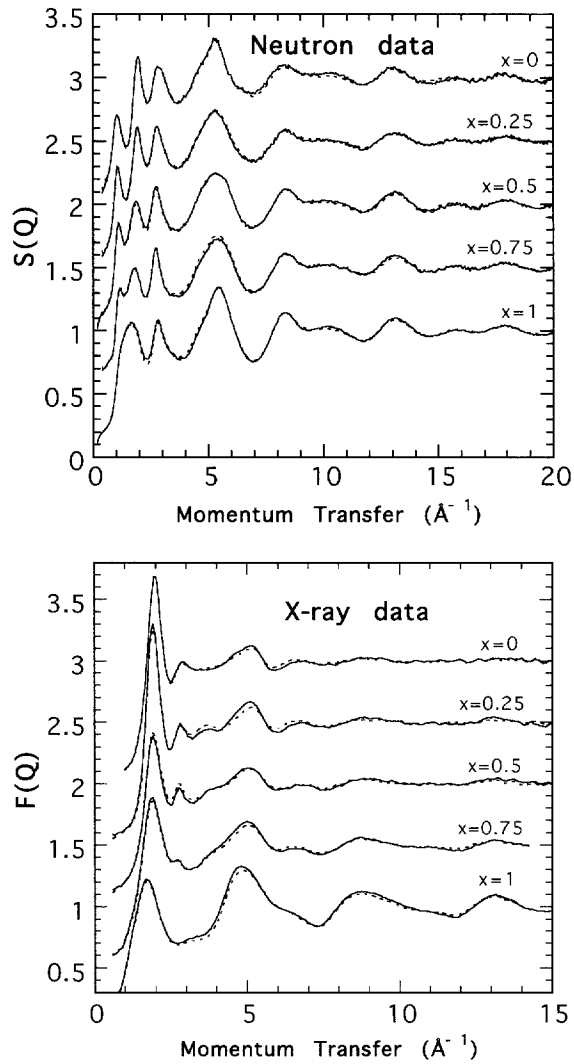

Fig. 2. Experimental neutron and X-ray structure factors (full lines) and computed neutron weighted and X-ray weighted structure factors (dashed lines) for the RMC configurations of the single and mixed alkali glasses $Li_xRb_{1-x}PO_3$. Consecutive curves are shifted by 0.5 for clarity.

Since these experiments have shown that the structure of meta-phosphate glasses consists of PO_4-tetrahedra sharing two corners and forming polymer like chains we let each phosphorous atom to be 4 coordinated by oxygen, 1/3 of the oxygen atoms to be two-coordinated by phosphorus (bridging oxygens), and 2/3 of the oxygen to be singly coordinated (non-bridging oxygens, NBO). In this way phosphate chains with 2 NBOs per PO_4-unit were obtained. The alkali ions coordinate to the NBOs of the PO_4 chains and provide weaker ionic links between the strongly bonded covalent chains [23].

To ensure that the alkali ions attain realistic bonding distances and coordination numbers to the oxygens we used a soft bond valence constraint for the ions to minimize the deviation from the expected valence sum, as described in Ref. 24. Furthermore, closest approach distances were used for all the different atomic pairs in order to avoid any unrealistically close atoms. These values were determined from the experimentally obtained pair correlation functions and tabulated ionic radii. The size of the simulation box, containing 4000 atoms for each composition, was set to satisfy the macroscopic density of the glass. The final RMC produced structural models of the five mixed alkali glasses were in excellent agreement with the experimental neutron and X-ray diffraction data, as shown in Fig. 2.

3. Bond Valence Analysis

The bond valence sum method has its roots in crystallography, where it is widely used as a way of determining the plausibility of crystal structure models [3-5]. The bond valence sum of a cation, M^+, may be expressed as

$$V = \sum_X s_{M^+-X^-}, \qquad (1)$$

where the contribution from adjacent anions, X^-, are commonly given by

$$s_{M^+-X^-} = \exp\left[\frac{R_0 - R_{M^+-X}}{b}\right]. \qquad (2)$$

The parameters R_0 and b are deduced from crystalline structures such that the bond valence sum of the monovalent Li^+ and Rb^+ ions in their equilibrium positions have a value close to the ideal $V_{ideal} = 1$. For this study, we have used the parameter set [25] $R_0 = 1.1745$, $b = 0.514$ for Li-O and $R_0 = 2.0812$, $b = 0.415$ for Rb-O. The pathways of ionic conduction through a solid should follow the path of lowest bond valence mismatch, $\Delta V = |V_{ideal} - V|$, corresponding to the energetically most favourable pathway. In crystalline solids, there is a direct relationship between the activation energy of ionic diffusion and the lowest bond valence mismatch for which the conduction pathways become infinite. For glasses there is no such simple

relationship since the structure shows too large variations, which make a determination of the lowest mismatch corresponding to the experimental E_σ difficult. In addition to this, the limited size of our model structures makes the lowest mismatch statistically uncertain. A more successful approach is to instead relate E_σ to the volume of the percolating cluster at a fixed value of the mismatch (in this study, we have used ΔV = 0.2 v.u.) for different glasses. The exact value of the chosen mismatch does not affect our results substantially, as we have previously shown [11]. To determine the conduction pathways, the glass structure is divided into ca. 4 million cubic volume elements (with a size of ≈ 0.2 Å) in which the bond valence mismatch is calculated for a hypothetical cation. The element is classified as accessible if the mismatch ΔV < 0.2 or if the sign of ΔV_{ideal}- changes within the element. The second criterion is added to reduce the effect of the limited resolution so that connections within the cluster are not overlooked. Accessible elements that share a common face or edge belong to the same cluster. If such a cluster percolates through the structure, it is considered to contribute to the dc conductivity of the glass. The volume of these percolating clusters relative to the total volume of the structure is given by the pathway volume fraction F.

4. Results

We have previously shown [26] that the experimentally determined E_s as well as the dc conductivity scales with the pathway volume fraction, F, and the mass of the mobile ion, m, as

$$A_1 + B_1 \cdot \left(F\sqrt{M}\right)^{1/3} = -\frac{E_\sigma}{RT} \quad (3)$$

$$A_2 + B_2 \cdot \left(F\sqrt{M}\right)^{1/3} = \log\left(\sigma T\sqrt{M}\right) \quad (4)$$

These results hold for all glasses that have been tested, including those in the present study, as long as the maximum threshold is reasonably realistic. This gives the possibility to predict the activation energy and the dc conductivity directly from structural models of glasses, see Fig. 1. The agreement between calculated and experimental values is, considering the large experimental errors in conductivity measurements of the lowest conducting glasses, fully satisfactory.

In Fig. 3, we show slices of the calculated percolating pathway clusters for Rb in $RbPO_3$ (3(a)), and the Li pathways in $LiPO_3$ (3(c)). Visual inspection of these pathway clusters alone, reveal some interesting properties. It is readily seen that the pathways in $LiPO_3$ have a larger volume and a more fine-structured network than those for the pure rubidium phosphate glass. Both these properties suggest a higher conductivity for Li ions in the pure lithium phosphate glass For the intermediate composition $Li_{0.5}Rb_{0.5}PO_3$, the pathways of both Li and Rb are shown in Fig. 3(b). In this case, none of the mobile ion clusters form a percolating pathway through the glass due to the blocking by unlike ions causing the pathway clusters to break up into smaller unconnected clusters. It is also clear from

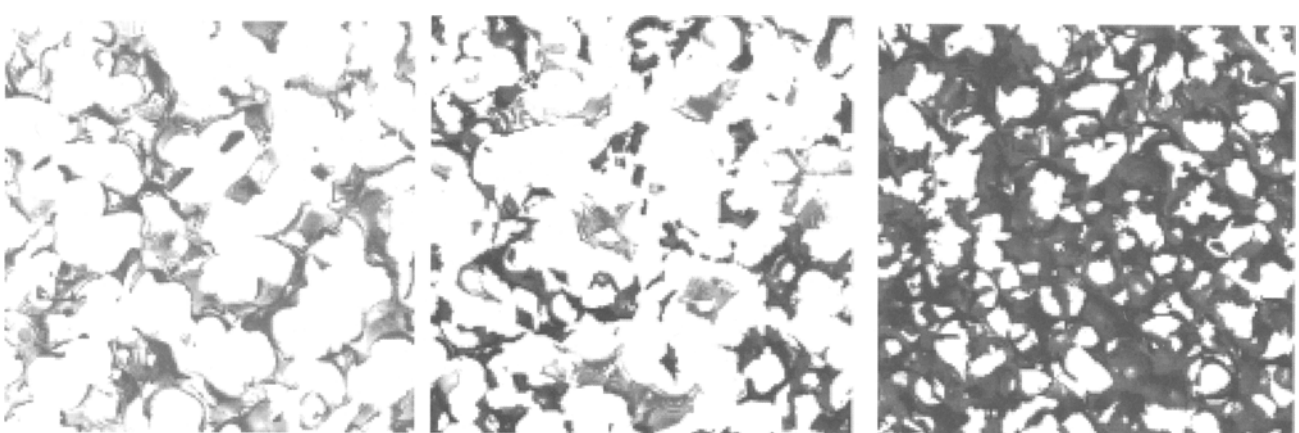

Fig. 3. Conduction pathways for Li^+ and Rb^+ ions in the glasses (a) $RbPO_3$, (b) $Li_{0.5}Rb_{0.5}PO_3$ and (c) $LiPO_3$. Li (Rb) pathways are shown as dark (light) isosurfaces for the bond valence mismatch threshold ΔV=0.2 valence units. The thickness of the displayed slices are 8 Å.

the figure that the lithium and the rubidium ions have distinctly different conduction pathways. The different pathways for Li and Rb are a consequence of the different sizes and polarisabilities of the Li and Rb ions resulting in the two having distinctly different local environments. Therefore there is a large energy mismatch for a Li to jump to a side that is well adapted to Rb and vice versa, as shown by molecular orbital calculations [27].

In order to further classify the structure of a conduction pathway, its dimensionality may be analyzed using the definition of dimension from fractal theory. The fractal dimension of mass is commonly defined as

$$n(R) \sim R^d, \tag{5}$$

where $n(R)$ is the average number of volume elements belonging to the same cluster within a radius R (or equivalently, the average mass of the part of the pathway cluster within the radius R), and d is the fractal dimension. Thus, plotting the log-log diagram of $n(R)$ vs. R as in Fig. 4 gives the dimensionality as the slope of a straight line fitted to the data points. Note that d only has its familiar meaning of fractal dimension if the straight line is fitted over a sufficiently large range of R. More detailed information on the pathway structure may be extracted if we instead investigate the local derivative of the logarithmic $n(R)$ vs. R curves,

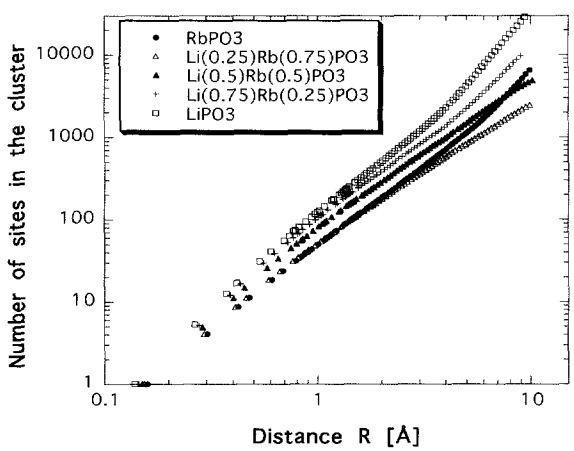

Fig. 4. Number of elements within radius R belonging to the pathway cluster, $n(R)$. The symbols given in the figure correspond to Li pathways in $LiPO_3$, $Li_{0.75}Rb_{0.25}PO_3$ and $Li_{0.5}Rb_{0.5}PO_3$, and Rb pathways in $RbPO_3$ and $Li_{0.25}Rb_{0.75}PO_3$. The fractal dimension of mass is obtained as the slope of the logarithmic representation of $n(R)$ vs. R.

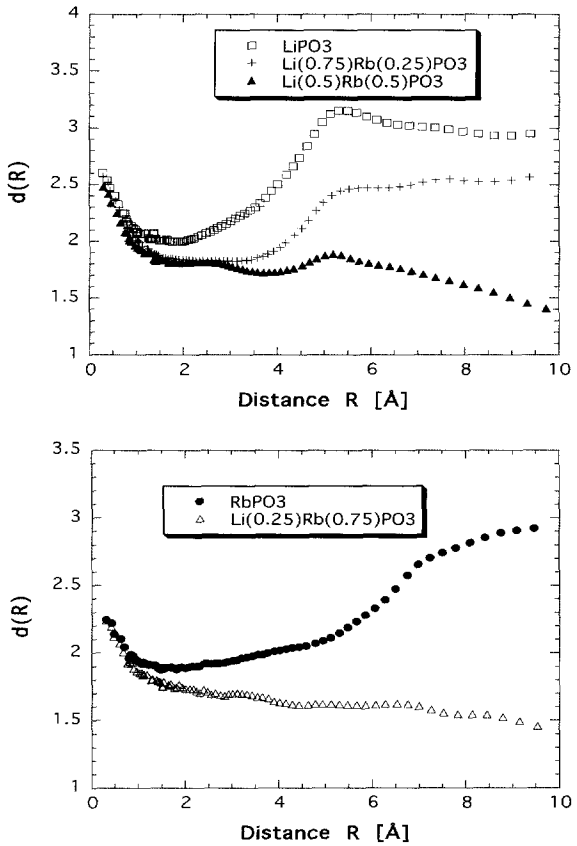

Fig. 5. $d(R)$ in $Li_xRB_{1-x}PO_3$ glasses. (a) $d(R)$ for percolating lithium pathways in the glass compositions $x = 1$ and $x = 0.75$, and the average $d(R)$ of the four largest clusters in the non-percolating $x = 0.5$ composition. (b) $d(R)$ for the percolating rubidium pathway in the glass composition $x = 0$, and the average $d(R)$ of the four largest clusters in the non-percolating $x = 0.25$ composition. The symbols correspond to the same glasses as in Fig. 4.

$$d(R) = R \frac{d}{dR} \log(n(R)) \tag{6}$$

In Fig. 5(a), these local derivatives are shown for the $Li_xRb_{1-x}PO_3$ compositions $x = 1$ and $x = 0.75$, for which there are percolating Li pathways, and $x = 0.5$, where no infinite pathway exists. In the pure $LiPO_3$ glass ($x = 1$), we can identify three regions;

1) In the range $R = 0$-1 Å the derivative approaches a value close to 3 as $R \rightarrow 0$, an expected result since the pathways have a finite thickness. As R increases, $d(R)$ decreases to values close to 2, indicating that the infinite pathway has locally a sheet-like structure.

2) In the region R = 2-3.5 Å there is a nearly linear increase in $d(R)$. This is probably due to branching of the pathways, resulting in a higher dimensionality of the cluster.
3) At 3.5 Å, the slope of $d(R)$ increases and $d(R)$ reaches a peak where $d(R$=5.4 Å) = 3.15.

As R approaches 10 Å we can see a slight increase in $d(R)$, which might correspond to the fact that we are now at roughly twice the characteristic length.

A $d(R)$>3 may seem puzzling, but it is important to note that here $d(R)$ is not the dimension of the pathway but rather the local slope of the logarithmic $n(R)$ vs. R curve. Fig. 6 shows a simple sketch of a pathway in 2 dimensions and the three proposed regions in $d(R)$. For $R \leq R_1$, the most local region, $d(R)$ starts at a value of 2 and drops below 2 when R becomes larger than the width of the pathway, and continues decreasing with increasing R as the pathway approaches one-dimension on the length scale of R_1. In the range $R_1 < R \leq R_2$, the branching region, $n(R)$ increases faster than linearly and thus the $d(R)$ will have a value > 1. As we enter the region of characteristic distance between the different parts of the pathway, $R_2 < R \leq R_3$, $n(R)$ will increase rapidly when R is large enough to include the neighbouring pathways marked (a) and (b) in the figure. $d(R)$, which approximately can be written as

$$d(R) = \frac{R}{\Delta R} \log \frac{n(R + \Delta R)}{n(R)} \qquad (7)$$

can thus reach large values and, depending on the exact structure of the pathway cluster, quite possibly >> 2, as it depends on the relative, and not the absolute, increase of $n(R)$. The peak at R = 5.4 Å in the Li ion pathway $d(R)$ is thus an indication of an ordering within the cluster with a characteristic distance of 3.5-5.5 Å between different clusters of the same pathway cluster.

Turning our attention to the x = 0.75 composition, we see a dramatic drop in $d(R)$ for all distances larger than 1 Å, indicating that a large part of the pathway cluster has been excluded by the addition of Rb ions. The region 2-3.5 Å is now nearly flat and thus the ions are more restricted in the number of directions to move. At 3.5-5 Å we see again the increase of $d(R)$ caused by the characteristic distance between neighbouring pathways of the same pathway cluster, but it has a significantly lower peak ($d(R)$~2.4) since several of the pathways in $LiPO_3$ are now blocked and therefore no longer parts of the percolating pathway cluster.

In the x = 0.5 composition, there is no longer any percolating cluster for Li, so $d(R)$ has been calculated as an average of the four largest clusters. Up to 2.5 Å $d(R)$ is close to that of the x = 0.75 composition, but as the distance increases, $d(R)$ decreases towards zero due to the limited extent in space of these clusters.

The pure rubidium phosphate glass, depicted in Fig. 5(b), exhibits the same general features as the $LiPO_3$ glass. There is an initial decrease of $d(R)$ in the region 0-1 Å and it reaches its minimum of ~1.9 at R = 1.5 Å. The nearly linear increase of $d(R)$ in the distance range 1.5-5 Å is again attributed mainly to the branching of the pathway cluster. Compared to the $LiPO_3$ glass, this region has a reduced slope and extends to longer distances in the $RbPO_3$ glass. At 5 Å, the slope of $d(R)$ increases again as we have now reached the characteristic distance between neighbouring pathways of the same pathway cluster. Both the slope of this region and the "peak" is significantly lower than that of the pure Li glass, suggesting a weaker correlation between the different parts of the pathway cluster. Fig. 5(b) also shows the average $d(R)$ for the four largest clusters in the x = 0.25 composition, where no percolating pathway exist. Like in the Li case, it follows the pure $RbPO_3$ in the region 0-0.7 Å. At higher R, $d(R)$ drops quickly, due to the effective blocking of the low-dimensional Rb pathways. The small peaks in $d(R)$ as R increases are features of the individual clusters

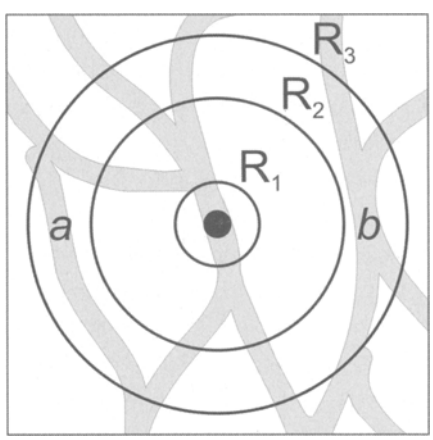

Fig. 6. Schematic illustration of conduction pathways and the three proposed regions of $d(R)$. $R < R_1$ is the most local region, $R_1 < R \leq R_2$ the branching region and $R_2 < R \leq R_3$ corresponds to the characteristic distance between neighbouring pathways of the same pathway cluster.

and thus do not reflect any general features of the cluster structures.

5. Discussion

We have here extended our previous study [11] of the local structure and dimensionality of the conduction pathways in mixed $LiRbPO_3$ glasses with a more detailed investigation of the dimensionality. The findings here confirm our previous report of relatively low dimensional pathways on a length scale < 4 Å, and complement them with foremost the observation that the most local structure (0-0.7Å) of the pathways is not substantially affected by the introduction of unlike ions to the single alkali ion phosphate glasses. This is in agreement with diffraction [12,17] and infrared absorption experiments [22], and further explains the experimental findings [28] that the MAE basically vanishes at high frequency ac conductivity.

Let us now turn to the difference between the Li and Rb pathways in the single alkali phosphate glasses. We can easily see that the dimensionality is consistently lower for the Rb glass, and not really reaching the dimensionality of Li until ~ 8 Å radius. The lower dimensionality reflects lower value of b for the Rb-O interctions, when compared to the Li-O interactions. The most interesting parts of the $d(R)$ curve is around the same length as the hopping distance for the mobile ions, ~2.8 Å for Li and ~3.9 Å for Rb [12]. Comparing these two regions of the two single alkali ion glasses, we see that Li has a higher dimensionality at the typical hopping distance than Rb and thus it would suggest both a higher conductivity due to more conduction paths, and also a higher resistance towards blocking of unlike ions. Another difference is the extent of the different regions in the two glasses. The branching region has a reduced slope in $RbPO_3$ but extends further (to 5 Å for Rb vs. 3.5 Å for Li), so the development towards higher dimensionality seems slower for the rubidium glass. The characteristic distances in the two glasses, 3.5-5.5 Å in Li and 5-7 Å in Rb, suggest that the Rb pathway structure has larger internal distances. This finding is consistent with data from neutron diffraction measurements [12] where the position, Q_1, of the first peak in $S(Q)$ roughly gives the correlation length, $r \approx 2\pi/Q_1$, between neighbouring PO_4 chains to ~3.7 Å in $LiPO_3$, and ~6 Å in $RbPO_3$. The correlation length regions also show a lower slope in $d(R)$ and a more diffuse peak in the Rb pathways. This difference indicates a weaker correlation between neighbouring pathways, as well as a fewer number of neighbouring pathways around any given pathway in the rubidium pathway structure of $RbPO_3$, compared to the case of lithium pathways in $LiPO_3$. It should be noted that the causes of increase in $d(R)$ in the two regions, here identified as branching and characteristic distance, are not readily distinguished from each other, and further investigations of the local pathway structure are needed to make a clear distinction between the branching region and the region corresponding to the characteristic distance between pathways. One possible technique is to use the concept of chemical dimension [see e.g. ref. 29]. The chemical dimension, d_l, can be defined in a manor similar to the
fractal dimension of mass,

$$n(l) \sim l^{d_l} \tag{8}$$

Here, $n(l)$ is the average number of elements in the cluster at a chemical distance $\leq l$, where the chemical distance is the shortest path within the pathway an ion can take between twovolume elements, in contrast to R in eq. (5) which is the Euclidian distance between the elements. d_l will show features of the cluster from our most local region and from the branching region ($0 \leq R \leq R_2$ in Fig. 6), but is insensitive to neighbouring pathways and can thus be used to analyse the branching region alone. We can, in line with eq. (6), define $d_l(l)$ as

$$d_l(l) = l\frac{d}{dl}\log(n(l)) \tag{9}$$

and through this obtain information on the dimensionality of the pathway, local to the ion. The rise in $d(R)$ when R is in the range of the characteristic distance between neighbouring pathways will not show up in $d_l(l)$ for those pathways that have a large chemical distance between them. Further investigations including an analysis of the chemical dimension are planed for the future.

Above, we have only addressed the blocking of pathways by unlike ions in our investigation of the mixed alkali effect, but it should be noted that, as we have previously reported [11], this is not the only reason for the dramatic drop in conductivity in the intermediate compositions. Even if the blocking effect is ignored, the predicted conductivity will be lower for the mixed glasses as e.g. the $Li_{0.5}Rb_{0.5}PO_3$ glass is not as well adapted to Li due to the lower concentration of Li ions.

This leads to local strains in the structure that affect the transport pathways in its environment. However, the blocking has by far the largest influence on the mixed alkali effect [11].

The approach towards an understanding of the MAE that has been presented here is based on static structural models of glasses where no relaxation, apart from the hopping of the mobile ions, is allowed. The successful explanation of the MAE using this approach implies that the site relaxation time in room temperature is slow compared to the residence and hopping time of the ion, and thus plays a limited role in the MAE. If the temperature is increased and the site relaxation time approaches the combined residence and hopping time of the ion, a site previously adapted for an A ion may rearrange in order to accommodate a B ion and in that way reduce the MAE. This is in agreement with experimental findings which show that the MAE decreases rapidly with increasing temperatures [28].

6. Conclusion

In conclusion, we have here elucidated the detailed structure of the conduction pathways in mixed alkali phosphate glasses calculated from static RMC produced structural models using the bond valence method. Our approach allows us to predict not only the conductivity of single mobile ion glasses, but also the mixed alkali effect. The findings are in agreement with experimental investigations, and show that the inclusion of unlike ions affects the dimensionality of the pathways on length scales larger than 1 Å, whereas the most local structure remains almost unchanged. The drop in conductivity for mixed compositions is mainly caused by a blocking of the pathways of both ions as Li and Rb have distinctly different pathways. This blocking can be very effective as the pathways have a relatively low dimensionality at the typical hopping distance of the mobile ions.

7. Acknowledgements

We thank C. Karlsson for providing us with conductivity data on the $Li_xRb_{1-x}PO_3$ glass system. J. S. is a Royal Swedish Academy of Sciences Research Fellow supported by a grant from the Knut and Alice Wallenberg Foundation. Financial support to J. S. from the Swedish Foundation for Strategic Research and to St. A. from the Deutsche Forschungsgemeinschaft is gratefully acknowledged.

8. References

[1] R.L. McGreevy, Nucl. Inst. Meth. In Phys. Res. A **354**, 1 (1995).

[2] R.L. McGreevy, J. Phys. Condens. Matter **13**, R877 (2001).

[3] I.D. Brown, The Chemical Bond in Inorganic Chemistry - The bond valence model(Oxford University Press, 2002).

[4] I.D. Brown, Acta Crystallogr., Sect. B: Struct. Sci. B **53**, 381 (1997); B **48**, 553 (1992).

[5] V. S. Urusov, Acta Crystallogr., Sect. B: Struct. Sci. B **51**, 641 (1995).

[6] J.O. Isard, J. Non-Cryst. Sol. **1**, 235 (1969).

[7] D.E. Day, J. Non-Cryst. Sol. **21**, 343 (1976).

[8] M.D. Ingram, Phys. Chem. Glasses **28**, 215 (1987).

[9] S. Balasubramanian and K.J. Rao, J. Non-Cryst. Solids **181**, 157 (1995).

[10] J. Habasaki, I. Okada and Y. Hiwatari, J. Non-Cryst. Solids **208**, 181 (1996).

[11] J. Swenson and St. Adams, Phys. Rev. Lett. 90, 155507 (2003).

[12] J. Swenson, A. Matic, C. Karlsson, L. Börjesson, C. Meneghini and W.S. Howells, Phys. Rev. B **63**, 132202 (2001).

[13] D.A. Keen and R.L. McGreevy, Nature **344**, 423 (1990).

[14] J. Wicks, L. Börjesson, R.L. McGreevy, W.S. Howells and G. Bushnell-Wye, Phys. Rev. Lett. **74**, 726 (1995).

[15] J. Swenson, L. Börjesson, R.L. McGreevy, and W.S. Howells, Phys. Rev. B **55**, 11236 (1997).

[16] Swenson, R. L. McGreevy, L. Börjesson, and J. D. Wicks, Solid State Ionics **105**, 55 (1998).

[17] J. Swenson, A. Matic, A. Brodin, L. Börjesson and W.S. Howells, Phys. Rev. B **58**, 11331 (1998).

[18] W.S. Howells, RAL-86-042, Rutherford Appleton Laboratory, Didcot, UK, 1986.

[19] C. Meneghini, F. Balerna, F. Boscherini, S. Pascarelli and S. Mobilio, J. Synchrotron. Radiat. **5**, 1258 (1998).

[20] C. Karlsson, C. Meneghini and J. Swenson, Phys. Rev. B **69**, 224209 (2004).

[21] R.K. Brow, C.C. Phifer, G.L. Turner and R.J. Kirkpatrick, J. Alm. Ceram. Soc. **74**, 1287 (1991).

[22] Jr. G. B. Rouse, P. J. Miller, and Jr. W. M. Riesen, J. Non-Cryst. Solids **28**, 193 (1978).

[23] B. Nelson and G. Exarhos, J. Chem. Phys. **71**, 2739 (1979).

[24] J. Swenson and St. Adams, Phys. Rev. B **64**, 024204 (2001).

[25] St. Adams, Acta Crystallogr., Sect. B: Struct. Sci. B **57**, 278 (2001).

[26] St. Adams and J. Swenson, Phys. Chem. Chem. Phys. **4**, 3179 (2002).

[27] T. Ushino, et al., J. Non-Cryst. Solids **146**, 26 (1992).

[28] C. Karlsson, A. Mandanici, A. Matic, J. Swenson, L. Börjesson, Phys. Rev. B **68**, 064202 (2003).

[29] A. Bunde, J. Dräger, M. Porto, in: Computational Physics, (K.H. Hoffmann and M. Schreiber, Eds.) Springer, Heidelberg, 1996, pp. 121-146.

Paper presented at the Patras Conference on Solid State Ionics - Transport Properties, Patras, Greece, Sept. 14 - 18, 2004.

Manuscript rec. Sept. 16, 2004; acc. Oct. 10, 2004.